Paper ID ICLASS06-125

NUMERICAL STUDY OF DIGITAL HOLOGRAPHIC MEASUREMENT OF DROPLET SIZE IN ATOMIZATION PROCESS

Shigeru MURATA [1], Yukinobu ANEZAKI [2] and Kenji KANEHARA [3]

[1]Kyoto Institute of Technology, murata@kit.jp
[2]Nippon Soken, Inc., YUKINOBU_ANEZAKI@soken1.denso.co.jp
[3] Nippon Soken, Inc., KENJI_KANAHARA@soken1.denso.co.jp

ABSTRACT This paper presents the technique of digital holography for the size measurement of small objects, such as fuel droplets in atomization process, and the measurement accuracy is evaluated by numerical simulation. Object images are reconstructed from an observed hologram image based on the technique of phase-shifting digital holography and they are digitally visualized with the information of relative phase of reconstructed light amplitude. The size of each reconstructed object is measured using the technique of Hough transform. The measurement accuracy of the present method is evaluated in numerical simulation for two different object models and the model with a simulation parameter of aspect ratio of ellipsoidal object. The performance test results for object width 5μm show that the RMS errors in depth position and object diameter are nearly constant up to the total number of objects 2000 for aspect ratio 1, and the length and width of ellipsoidal objects can be measured within error ratio 20% up to aspect ratio 3 for the total number of objects 1000. It is also shown that object images can be clearly reconstructed even for higher number density of objects by using the information of relative phase of light amplitude as compared with the conventional information of light intensity.

Keywords: Digital Holography, Spray Measurement, Droplet Size, Phase Shifting, Numerical Simulation

1. INTRODUCTION

In spray measurement, the point-measuring techniques for particle measurement such as well-known phase Doppler particle analyzer (PDPA), shadow Doppler method and Fraunhofer diffraction intensity technique have been widely used to know the size of liquid droplets in spray. However the phenomenon of liquid atomization should be spatially analyzed as the behavior of liquid jet or droplets in 3D space. From this point of view, holographic method [1] is advantageous to the point-measuring techniques because it enables us to realize the spatial and instantaneous structure of spray.

In recent years, digital holography [2][3] has been recognized as a powerful tool for analyzing the small objects distributed in three-dimensional space, such as tracer particles used in flow visualization or particle image velocimetry and tiny air bubbles traveling in water flow. This technique has some striking advantages as compared with the conventional holography. The first one is that the off-line process of hologram development is not required because hologram patterns are electrically captured with a CCD or CMOS camera and they are converted directly to a digital image. The second one is that the 3D information of the small objects recorded on the digital hologram image can be numerically extracted on a PC by reconstructing the distribution of light wave passing through the hologram, based on the theory of wave optics. Though the spatial resolution of real hologram plate should be about 1000-7000(line/mm) for the purpose of fine image reconstruction of 3D objects, data mining can be carried out from a digital hologram image with a certain level of measurement accuracy.

In this paper, the technique of digital holography has been developed for accurately measuring the small objects distributed in 3D space with higher number density. The measurement accuracy of the technique is evaluated by numerical simulation using the artificial hologram images for some models of small objects distributed in 3D space.

2. MEASUREMENT PRINCIPLE

2.1 Digital Holography

In digital holography, the information of the objects distributed in 3D space is recorded with an electric imaging device, for example CCD and CMOS cameras, and it is reconstructed numerically on a digital computer. Figure 1 illustrates the optical setup for digital holographic measurement. The optical observation system consists of laser, spatial filter, laser collimating lens and an electronic camera without a camera lens and these are set up in line. Spray is injected into the region between the collimating lens and the electronic camera. If a time series of digital hologram images is captured with a high-speed video camera, traveling speed of droplets may be measured for the case with low number density.

The numerical image reconstruction is carried out based on the Fresnel diffraction formula in wave optics using the digital images of observed hologram patterns. In our previous papers [4]-[6], the input information to the Fresnel diffraction formula was the transparency function on

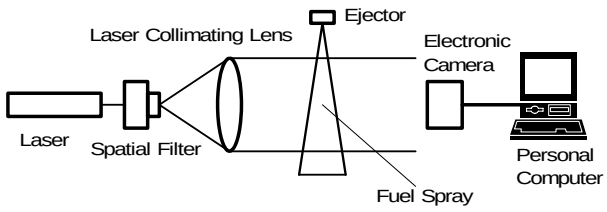

Fig.1 Measuring system.

hologram plane that expresses the hologram pattern recorded on a digital image and the output information was the light intensity at a certain depth coordinate perpendicular to hologram plane. However, since the reconstructed object image is enlarged along the depth direction and then the images are interfered to each other to be noisy and degraded, so it is difficult to measure some object quantities with accuracy, such as object diameter and object position, from the light intensity distribution in 3D space. Furthermore, according to the technique of phase-shifting digital holography [7] [8], the light amplitude on hologram plane is taken as an input information to the formula to improve the quality of reconstructed images.

Then, the Fresnel diffraction formula employed in the present paper can be represented by

$$h_z(x_z, y_z, z; h_d(x,y)) = \frac{1}{j\lambda z}\int_{-\infty}^{\infty}\int_{-\infty}^{\infty} h_d(x,y)\, e^{j\frac{2\pi}{\lambda}\left[z+\left\{(x-x_z)^2+(y-y_z)^2\right\}/2z\right]} dxdy, \quad (1)$$

where h_z is the light amplitude on image plane (x_z,y_z) and h_d is the light amplitude on hologram plane (x,y), that can be computed with four different hologram images obtained by changing the phase of reference light wave at an interval of quarter-wavelength. z, λ and j denote the coordinate originating from hologram plane and perpendicular to it, wavelength of illuminating light wave and the imaginary unit, respectively.

In general, the light intensity $|h_z|^2$ is computed for each observed hologram image at an arbitrary z-coordinate to confirm the reconstructed images. However, relative phase distribution is employed to show the reconstructed images and detect some quantitative information on target objects from the distribution, as described in the above. The procedure of computing the relative phase is explained in the following. Since the light amplitude h_z is expressed as complex number by Eq.(1), the phase difference ϕ between the light amplitude h_z and that of illuminating light wave on the background of reconstructed image h_0 can be obtained, as follows:

$$\phi(x_z, y_z, z) = \cos^{-1}\left\{\frac{\mathrm{Re}(h_z)\,\mathrm{Re}(h_0)+\mathrm{Im}(h_z)\,\mathrm{Im}(h_0)}{\sqrt{\mathrm{Re}(h_z)^2+\mathrm{Im}(h_z)^2}\sqrt{\mathrm{Re}(h_0)^2+\mathrm{Im}(h_0)^2}}\right\}, \quad (2)$$

where Re and Im express the real and imaginary parts of complex number, respectively. The relative phase defined by Eq.(2) is assigned to zero for the background at any depth coordinate z and $\pm\pi$ around the edge of target objects in the same way as light intensity distribution. Then the relative phase distribution can be converted to a digital image using the following equation

$$I_p(x_z, y_z, z) = G_{\max} - \left| G_{\max}\frac{\phi(x_z, y_z, z)}{\pi}\right|. \quad (3)$$

In this equation, $G_{\max}$ denotes the total number of possible gray levels at each pixel and it is given the value 256 for 8bit digital image, for example.

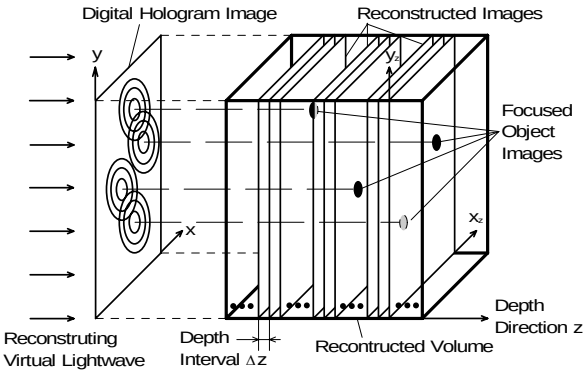

Fig.2 Numerical image reconstruction.

2.2 Object Measurements

Figure 2 depicts the concept of numerical image reconstruction based on Eqs.(1)-(3). Image reconstruction is carried out at a depth interval Δz over the range from $z_{\min}$ to $z_{\max}$ to construct the full-volume of relative phase in measuring region. In the volume, target object images can be clearly and locally reconstructed around the same z-coordinate as the corresponding true object depth. First, the volume of relative phase is binalized with a threshold I_{th} to detect the clusters of black pixels adjacent to each other,

$$I_b(x_z, y_z, z) = \begin{cases} 1 & \text{for } I_p(x_z, y_z, z) \le I_{th} \\ 0 & \text{for } I_p(x_z, y_z, z) > I_{th} \end{cases} \quad (4)$$

and then each cluster of the pixels with I_b=1 is labeled to distinguish it from the other clusters,

$$L_b(x_z, y_z, z) = L_0 \quad \text{for Label Number } L_0\,. \quad (5)$$

The threshold I_{th} is given by using the discriminant analysis method [9] that is a useful technique to automatically determine the value of threshold from a gray level histogram.

Object measurement is performed using the technique of Hough transform [10] in the present method. Hough transform is a useful technique in image processing for line-fitting to the target pixels located in line. Figure 3 illustrates the basic concept of Hough transform. The coordinates of each target pixels (x,y) is transformed into the coordinates (ρ,θ) as shown in Fig.3. In this study,

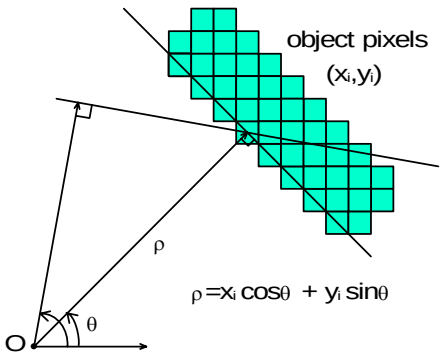

Fig.3 Object measurement using Hough transform.

changing θ at an interval of 1deg, the standard deviation of ρ, denoted by σ_ρ, is computed for each θ and then object width W and object length L are given by

$$W = 4 \times \underset{\theta}{\mathrm{Min}}(\sigma_\rho(\theta)) \,, \qquad L = 4 \times \underset{\theta}{\mathrm{Max}}(\sigma_\rho(\theta)) \,, \tag{6}$$

respectively. Furthermore, the position of each pixel cluster in 3D space can be given by taking average of the coordinates of the target pixels belonging to the corresponding cluster.

3. NUMERICAL SIMILATIONS

3.1 Object Models

In numerical simulation, the performance of the present technique is evaluated for the measurement accuracy of droplet size, depth position and the computing time. Assuming that each droplet can be expressed by a circular or elliptic disk for simplicity that is a target object, artificial hologram images are made for a various combinations of simulation parameters, for examples, number density of objects, depth range and object size. Since the reconstructed object image is much affected by those of neighboring objects for the case with higher number density of objects, one objective of this paper is to focus on the lower limit of object spacing to which the present technique can be applied with accuracy. Figure 4 illustrates the two object models used for performance test in this simulation. For the total number of objects N_p, the positions in 3D space for half of the objects $N_p/2$ are first determined at random with uniform random numbers, and then those of the other half of them are given by shifting the predetermined objects by δz along z-axis or by δx along x-axis. Model A is the object model with the object shift δz and Model B is that with the shift δx. Furthermore the positions of all the objects are determined completely at random without spatial shifting in Model C.

In all the models, aspect ratio R_a is a simulation parameter defined as

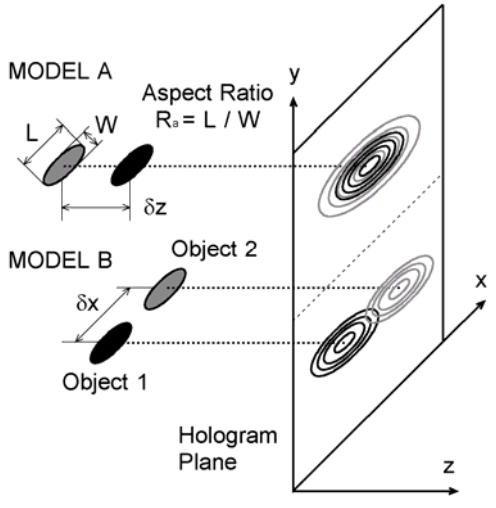

Fig.4 Object models for performance tests.

$$R_a = L / W \,, \tag{7}$$

where L and W denote the major and minor axes of an elliptic disk, respectively, and L also expresses the object length and W does the object width in object measurement.

3.2 Reliability of Image Reconstruction

This section describes the reliability of the reconstructed relative phase distribution for object measurements. In this paper, simulation parameters are set as summarized in Table 1.

Table 1 List of simulation parameters.

Number of objects N_p	500, 1000, 2000
Object width(μm) W	5,10
Object length(μm) L	$R_a \times W$
Aspect ratio R_a	1,2,3,4,5
Spatial shift δx	0,4,8,12,16,20
Spatial shift δz	5,10,15,20

A digital hologram and reconstructed images are composed of 512×512 pixel with 8bit gray-level resolution. The size of one pixel of a CCD or CMOS element is assigned to 2μm that is supposed to be the lower limit of the pixel size at the present day and the measuring range in depth is fixed at 10mm in this simulation. Image reconstruction is performed with the depth interval Δz=2μm.

Figure 5 compares the given true object positions on x-y plane with the projection image obtained by projecting all the reconstructed images of relative phase onto the x-y plane for the Model C with aspect ratio 1. Though the projection image is for the highest number density of objects 2000 in the present paper, it can be seen from Fig.5 that there is little difference between the two images in Fig.5 and each object is clearly reconstructed against the background without the interaction to the other object images.

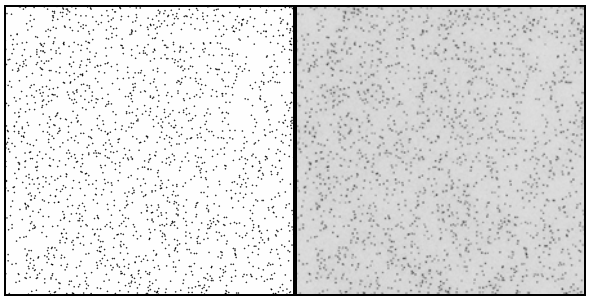

(a) True object positions (b) Projection image

Fig.5 Reliability of reconstructed object images.
(N_p=2000, R_a=1)

4. MEASUREMENT RESULTS

4.1 Effect of Object Spacing

This section examines the influence of object spacing on the measurement accuracy of the present method using Models A & B for the case with aspect ratio 1 and object diameter 5μm. Figure 6 shows the number of the detected objects for the given true number density 500. For Model A, the number of detected objects levels off at about 220 that corresponds to about half of the true one. This implies that the images of some object pairs are united to each other along *z*-axis and then the number of objects is undercounted because the reconstructed object image is enlarged along *z*-axis, as described above. Though the number will increase up to the true one if δz increases, the lower limit of spatial spacing for correct object identification is much dependent on object size. In the test with Model B changing δ*x*, the number of the detected objects is also about 220 for small δ*x* and it increases at δ*x*=10μm. It is found that the objects adjacent to each other can be distinguished on a spatially fine digital image if the spacing within *x*-*y* plane is more than twice object diameter.

Figure 7 shows the RMS error in diameter obtained for the same models as employed in Fig.6. The RMS error attains to 0.3μm for larger spatial spacing δ*x*. However it extremely increases up to 1μm for δ*x*=5μm because the images of some object pairs are partly overlapped to each other, and this corresponds to the result of Fig.6 in which the number of detected objects decreases for δ*x*=0 and 5μm. On the other hand, the RMS error is nearly constant for Model A, except for δz 20μm, in the same way as shown in Fig.6. Since δ*x* is assigned to 0μm, so the reconstructed images of objects adjacent along *z*-axis are completely overlapped and the object size is not overestimated. Hence the RMS error is as low as those for Model B with larger δ*x*.

Next, Figure 8 indicates the influence of the total number of objects recorded on one hologram image on the RMS errors in depth position and object diameter for (δ*x*, δz)=(0μm, 20μm). Both of the errors are nearly constant for any numbers of objects. The error in depth position is about 7μm for the depth range of 10mm and that in diameter is about 0.5μm. It is expected that the present method can be applied to the case with the number of objects more than 2000.

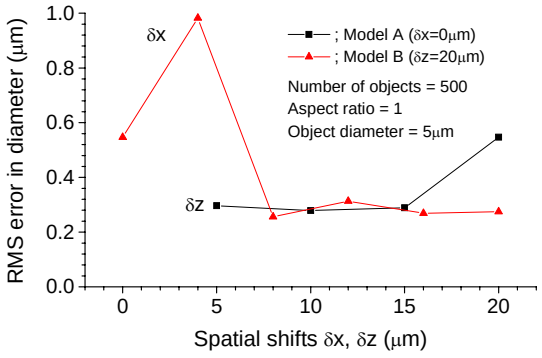

Fig.7 Change of RMS error in diameter with spatial shifts δx, δy.

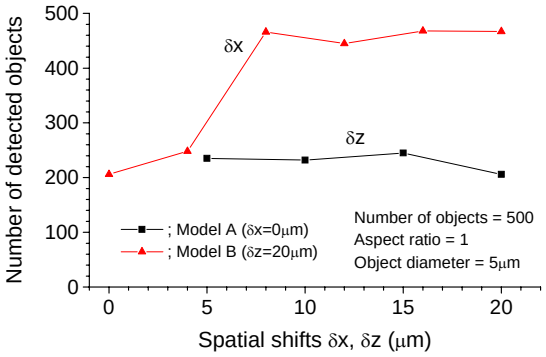

Fig.6 Change of number of detected objects with spatial shifts δx, δy.

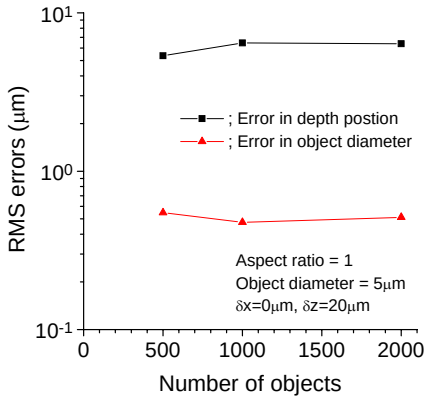

Fig.8 Influence of number of objects on RMS errors.

4.2 Effect of Aspect Ratio

The performance test results for different aspect ratios are shown in this section to examine the feasibility of the present method in the measurement of deformed droplets such as fuel spray in atomization process.

Figure 9 depicts samples of reconstructed object images for aspect ratios 1 to 5 and minor axis of object 5μm. It is easily seen that the object images have high contrast to the background. Next, the number of detected objects is compared in Fig.10 among five different aspect ratios and among three different numbers of objects. In general, it is a little difficult to determine the threshold for binarization for the images with different gray level histograms. In the

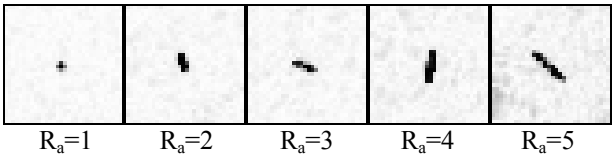

Fig.9 Samples of reconstructed object images for five different aspect ratios.

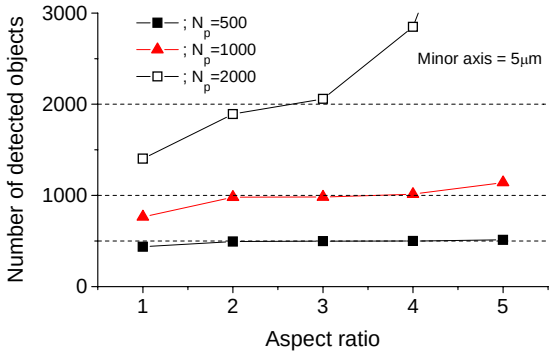

Fig.10 Number of detected objects.

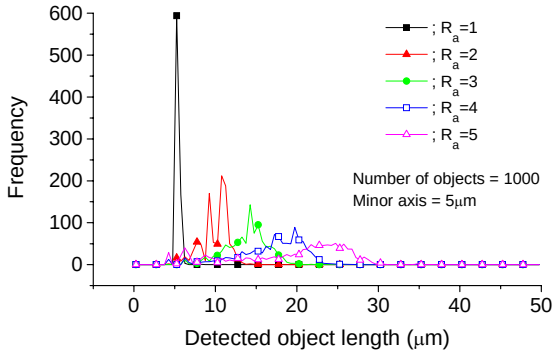

Fig.11 Histogram of detected object length.

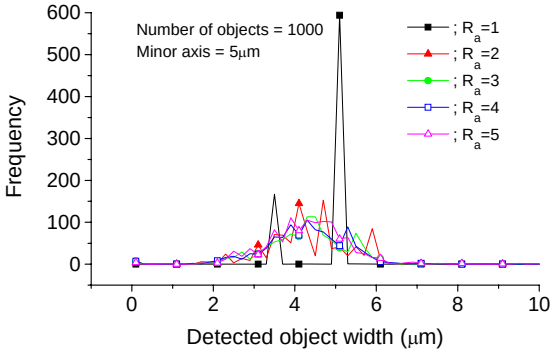

Fig.12 Histogram of detected object width.

present method, the discriminant analysis method is successfully used because the number of detected objects are nearly equal to the given number of objects N_p except for the cases with N_p=2000 and aspect ratio R_a larger than 4. For aspect ratio 1, the number of detected objects is lower than the true one for any N_p, but this will surely and easily be improved by adjusting the threshold interactively. However the results for N_p=2000 and aspect ratio larger than 4 can not be improved only by changing the threshold because a reconstructed object image is divided into some parts of the object and hence the number of objects are overestimated. The occurrence of the image division is much dependent on the occupancy ratio of objects projected

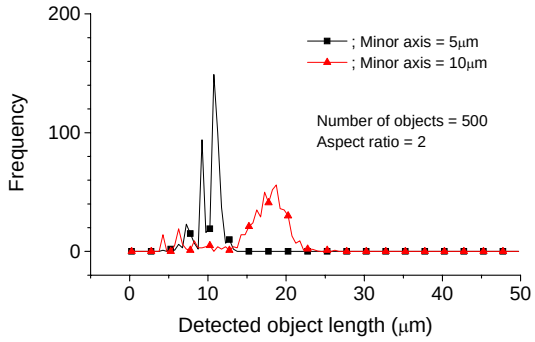

Fig.13 Comparison of histogram of object length between two different minor axes.

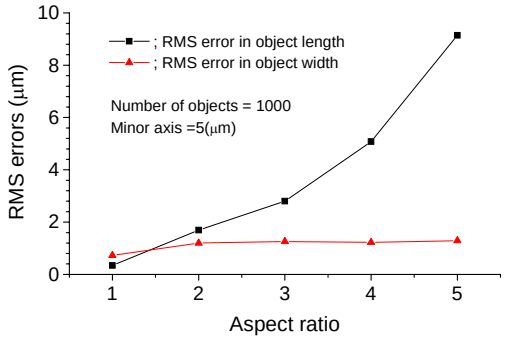

Fig.14 Relation between RMS errors and Aspect ratio.

onto *x-y* plane. For instance, the hologram image for N_p=2000 and R_a =5 has the same occupancy ratio as that for N_p=10000 and R_a =1.

Figures 11-12 show the histograms of detected object length and object width for the number of objects 1000 and minor axis 5μm, respectively. It is shown in Fig.11 that the histogram for aspect ratio 1 has a striking peak around 5μm that is the given true length and the histogram is lower and wider as aspect ratio is larger. On the other hand, as shown in Fig.12, the histogram of detected object width does not change exceedingly, though the histogram for R_a =1 has a steep peak in the same way as that of object length.

The influence of minor axis of elliptic object on measurement accuracy is demonstrated in Fig.13. The number of objects is 500 and aspect ratio is fixed at 2, and the histogram of detected object length is shown for the two different minor axes, 5μm and 10μm. From Fig.13, it is found that the present method presents good results even though the peak of the histogram moves to smaller region by about 1 μm.

Finally, the correlation between RMS errors and aspect ratio is shown in Fig.14. The RMS error in object width levels off over the range of aspect ratio from 1 to 5, and this is consistent with the results indicated in Fig.12. The RMS error in object length increases with increasing aspect ratio, however the length of ellipsoidal objects can be measured within error ratio 20% up to aspect ratio 3 for the total number of objects 1000.

4.3 Discussion

This section discusses the computing time required for processing one hologram digital image and the possible size of measuring region handled by the present method.

A personal computer with the Intel Pentium 4 CPU of 3.4GHz and the 4GB RAM was used in the present numerical simulations. Since the depth range was fixed at 10mm and the depth interval for image reconstruction Δz was assigned to 2μm, so 5001 reconstructed images had to be computed for one hologram image. It requires about 3sec to computing one image of 512×512 pixel in the present method. Though our program may be tuned up for saving processing time, it will take about 20 min to complete the processing of one hologram image. However the computation of reconstructing images can be done completely in parallel and hence the computing time will be surely reduced much by using a parallel processor or the computing system with a multi-core CPU. The processing of object measurement in the reconstructed volume does not require much computing time, for example less than 30 sec for one hologram image.

In the observation system shown in Fig.1, image magnification is given the value 1 because a camera lens is detached from the camera body and the laser beam directly illuminates the electronic device for image pick-up. Magnification can be changed with some lenses, but it is recommended not to use them for obtaining clear hologram patterns. The size of electronic device, such as CCD and CMOS, has recently become large up to about 35×25mm in the development of professional digital camera, so the size of measuring region is expected to be enlarged to measure the standard size of flow field in experiment.

5. CONCLUSION

This paper presented the technique of digital holography for the size measurement of small objects and the measurement accuracy was evaluated by numerical simulation. The reconstructed images were greatly improved by employing the technique of phase-shifting digital holography and the information of relative phase of reconstructed light amplitude to accurately measure the information of small objects such as object position and size. Evaluating the measurement accuracy of the present method with three different objects models, it was seen that the RMS errors in depth position and object diameter were nearly constant up to the total number of objects 2000 for aspect ratio 1, and the length and width of ellipsoidal objects could be measured within error ratio 20% up to aspect ratio 3 for the total number of objects 1000.

This research was partly supported by a Grant-in-Aid for Scientific Research (C) number 17560148 from the Japan Society for the Promotion of Science and by Mitutoyo Association for Science and Technology (MAST) in 2005 and 2006.

NOMENCLATURE

G_{max}	Number of possible gray levels on a digital image	
h_d	Light amplitude on hologram plane	
h_z	Light amplitude on image plane	
h_0	Light amplitude of reconstructing light wave on image plane	
I_b	Gray level of a binary image	
I_p	Gray level of a image of relative phase	
I_{th}	Threshold for binarization	
j	Imaginary unit	
L	Object length	[μm]
L_b	Label distribution in a reconstructed volume	
L_0	Label number	
N_p	Total number of objects recorded on one hologram image	
R_a	Aspect ratio of an ellipsoidal object	
W	Object width	[μm]
x, y	Cartesian coordinates on hologram plane	[μm]
x_z, y_z	Cartesian coordinates on image plane	[μm]
z	Depth coordinate perpendicular to a hologram plane	[μm]
δx	Spatial shift of objects along x-axis	[μm]
δz	Spatial shift of objects along z-axis	[μm]
Δz	Depth interval for image reconstruction	[μm]
λ	Wave length of light wave	[μm]
ρ,θ	Polar coordinates for Hough transform	
σ_ρ	Standard deviation of ρ for each cluster of pixels	[μm]
ϕ	Relative phase	[rad]

REFERENCES

1. Anezaki, Y., Shirabe, N., Kanehara, K. and Sato,T., 3D Spray Measurement System for High Density Fields Using Laser Holography, Proc. SAE 2002 World Congress & Exhibition, Paper No.2002-01-0739, 2002.
2. Schnars, U., Kreis, T. M. and Juptner, W. P. O., Direct Recording of Holograms by a CCD Target and Numerical Reconstruction, Applied Optics, Vol.32, pp.179-181, 1994.
3. Kreis, T. M. and Juptner, W. P. O., Principles of digital holography, Fringe'97, Berlin: Akademie Verlag GmbH, pp.353-363, 1997.
4. Murata, S. and Yasuda, N., Potential of Digital Holography in Particle Measurement, Optics & Laser Technology, Vol.32, pp.567-574, 2000.
5. Murata, S. and Yasuda, N., Development of Full-volume Digital Holography for Particle Measurement, Optical methods and data processing in heat and fluid flow (Eds. Greated, C. et al.), Professional Engineering Publishing, pp.69-77, 2002.
6. Murata, S., Morihara and T., Yamaguchi, T., Dynamic Measurement of Gas Bubbles in 3D Space by Means of Full-volume Digital Holography, CD-ROM Proceedings of International Conference on Multiphase Flow, Paper No.136, 2004.
7. Matoba, O., Naughton, T. J., Frauel, N., Bertaux, N. and Javidi, B., Real-time Three-dimensional Object Reconstruction by Use of a Phase-encoded Digital Hologram, Applied Optics, Vol.41, pp.6187-6192, 2002.
8. Awatsuji, Y., Sasada, M. and Kubota, T., Parallel Quasi-phase-shifting Digital Holography, Applied Physics Letters, Vol.85, pp.1069-1071, 2004.
9. Ohtsu, N., Discrimination and Automatic Adoption of Threshold Based on Least Square Standard, Transaction of the Institute of Electronics, Information and

Communication Engineers, Vol.J63-D, No.4 pp.349-356, 1980.
10. Pitas, I., Digital Image Processing Algorithms, Prentice Hall, 1993.